2016-01-01

DFT Study On The Structure And Properties Of VSc2N@c68

Surendra Bhatta
University of Texas at El Paso, sbhatta@miners.utep.edu

DFT STUDY ON THE STRUCTURE AND PROPERTIES

OF $VSc_2N@C_{68}$

SURENDRA BHATTA

Master's Program in Physics

APPROVED:

Tunna Baruah, Ph.D., Chair

Rajendra Zope, Ph.D.

Mahesh Narayan, Ph.D.

Charles Ambler, Ph.D.
Dean of the Graduate School

Dedication

To all my family members

DFT STUDY ON THE STRUCTURE AND PROPERTIES OF $VSc_2N@C_{68}$

by

SURENDRA BHATTA, Master's Degree

THESIS

Presented to the Faculty of the Graduate School of

The University of Texas at El Paso

in Partial Fulfillment

of the Requirements

for the Degree of

MASTER OF SCIENCE

Department of Physics

THE UNIVERSITY OF TEXAS AT EL PASO

August, 2016

Acknowledgements

In the process finalizing my thesis I would like to thank all those people who made this thesis possible and an unforgettable experience for me.

First of all, I would like to express my deepest sense of Gratitude to my supervisor **Dr. Tunna Baruah**, who offered her continuous advice, sincere attention and encouragement throughout the tenure. I thank her for the systematic guidance and effort she put into training me in the scientific field.

I would like to thank to **Dr. Rajendra Zope** for his unconditional co-operation and guidance.

I cannot proceed forward without praising Mr. **Shusil Bhusal,** without his help this thesis would not be up to the mark. Similarly, **Dr. Luis Basurto, Dr. Yoh Yamamoto** and all the members of electronic structure lab really are creditworthy for the lots of thanks.

Abstract

A computational study on the structure and electronic properties of the $VSc_2N@C_{68}$ molecule was carried out using the density functional theory. This molecule is based on the recent report on the synthesis of the $VSc_2N@C_{80}$ and $V_2ScN@C_{80}$ fullerenes. The $Sc_3N@C_{68}$ is also a stable endohedral fullerene that has a cage with fuse pentagonal rings. The doping by a V atom changes the structure as well as the spin state of the Sc3N@C68 from S=0 to S=1 state. Since the C_{68} has 6332 isomers, we have carried out an extensive search for the lowest energy structure of the C68 in several anionic structures: -2, -4, -6. The first screening of the anionic structures was done using PM6 methods. The lowest 300 isomers from this set was chosen, the endohedral fullerene was built with three different orientations of the endohedral unit and further optimized. The final 13 lowest energy structures were optimized at the DFT level. This extensive search showed that the lowest energy isomer of $VSc_2N@C_{80}$ differs from that of the $Sc_3N@C_{68}$ structure. The lowest energy isomer has three fused pentagons on the carbon cage. The isomers are found to be distinct with an energy difference of 0.46 eV between the two lowest isomers. The presence of the V leads to a S=1 state. The energetics show that the $VSc_2N@C_{68}$ can also be a good electron acceptor and is chemically stable. The calculated absorption spectra can help in characterization of the molecule in experiment.

Table of Contents

List of Tables

List of Figures

Chapter 1: Introduction

1.1 Fullerene: its discovery and properties

The discovery of the fullerene or the C_{60} molecule can be described as an epic moment in chemical and physical science not because of the applications of C_{60} but rather due of the developments in the area of nanotechnology that perhaps would not have occurred if C_{60} was not discovered. Also known as Buckminster fullerene named after Richard Buckminster Fuller or simply referred to as Bucky ball, the C_{60} was first identified by a group of scientists that included Richard Smalley, Robert Curl, and Harry Kroto at Rice University, Houston in 1985. [1,2] The group evaporated graphite by lasers, which produced extremely high temperature and as the vapor cooled the evaporated atoms formed clusters. The cooled vapor was analyzed through a mass spectrometer which showed high peaks for C_{60} accompanied by a smaller peak for C_{70}. The analysis by Kroto led to the identification of the structure of the C_{60} molecule as a truncated icosahedron with 20 hexagons and 12 pentagons forming a closed cage structure. [3] This was completely new form of carbon at the time and led to a flurry of studies on carbon nanostructures such as nanotubes which resulted in further developments in nanotechnology. Later the existence of other carbon cages containing 20 to hundreds of carbon atoms were discovered. [4] The carbon cages, which are also known as fullerenes, contain hexagonal and pentagonal rings forming closed structures. Each fullerene can have a large number of isomers, which can be generated by the permutation and combinations of pentagons and hexagons. However, the number of stable isomers for various sizes of fullerenes under standard conditions are quite few.

The carbon atoms in the C_{60} fullerene are sp^2 hybridized. In the absence of any strain, a planar sheet of sp^2 bonded carbon atoms will form a hexagonal lattice as in graphene. The presence of pentagons introduces curvature of the structure forming a closed cage. [5] The carbon atoms in the C_{60} fullerene form a strong network of sigma bonds surrounded by a layer of pi-electrons. While the C_{60} has a highly symmetrical soccer ball structure, the structures of other carbon cages have lower symmetry depending on the number of atoms. The C_{60} fullerene has a high energy gap (1.8 eV) [6] between its highest occupied molecular orbital (HOMO) and lowest unoccupied molecular orbitals (LUMO). The HOMO is 5-fold degenerate and the LUMO is 3-fold degenerate. [7] The HOMO to LUMO optical transition is symmetry forbidden. The fullerenes absorb mostly in the UV-visible region [8]. They also exhibit strong non-linear optical effects that arises from the delocalized pi-electrons. It is chemically stable and can also undergo cyclo-addition reactions mostly at the junction of two hexagons. Such reactions allow to develop various C_{60} derivatives with desirable properties e.g. derivatives that have lower absorption band or higher solubility. [9,10]

The C60 fullerene can also aggregate to form solid in an FCC lattice at room temperature. When intercalated with alkali atoms, the C_{60} solid is known for its superconducting properties [11]. The C_{60} fullerene also has high electron mobility and combined with its high electron affinity it poses as a good electron acceptor for solar cells [12]. The other possible applications are in hydrogen storage, bio-medical applications such as for drug delivery, as anti-oxidants etc. [13,14]

1.2 Endohedral Fullerene

Immediately after the discovery of Fullerene it was proposed that Fullerene can encapsulate some atoms inside it because of its completely closed cage nature. [15] The C_{60} has a diameter of

7 to 10 Å, which is large enough to accommodate an endohedral atom or molecule. Soon after the discovery of C_{60} in 1985, the La@C_{60} was also discovered in mass spectrum [16]. However, the amount of yield and purification of the soot from laser vaporization of the graphite electrodes doped with metals hindered the progress. The mass production of the fullerene started after Huffman and Krautchmer developed the arc-discharge method for mass generation of fullerene [17, 18]. The phenomena of the formation of endohedral fullerene takes place in different ways. The one way that takes place in twos steps first when the endohedral unit collides with fullerene cage, should absorb and redistribute a good part of the kinetic energy from cage to ensure that the ions have enough energy to break the cage. It allows the entering of unit. Then, in second step it should enter inside in such a way without having sufficient kinetic energy left to escape. This is also known as ion implantation method. The yield of endohedral fullerene is low. Next way to form endohedral fullerene is arc-discharge and laser evaporation method. In this method doped graphite are laser evaporated to produce. [19] Apart from encapsulation of metal atoms, noble gas atoms from He to Kr and even non-metal atoms such as N or P were also encapsulated within a carbon cage [20,21,22,23]. The focus was on isolating a single specie of endohedral fullerene. La@ C_{82} was the first isolated one found in 1991 [24] followed later by various M@C_{82} clusters with M=Y, Sc, Ca, Sr, Ba, and Ce-Lu [25,26,27,28]. Such endohedral structures are characterized by charge transfer from the encapsulated metal atom to the carbon cage forming a salt of the type $M^{+n}C_{2m}^{-n}$. For example, 3 electrons are transferred from the La to the C_{82} cage forming $La^{+3}C_{82}^{-3}$. Steric effects prevent the dissociation of the salt. The early studies on the La encapsulating fullerenes also noted the lack of La@C_{60} and La@C_{70} species. On the other hand, various Sc containing compounds were

noted such as $Sc@C_{82}$, $Sc_2@C_{78}$, $Sc_2@C_{82}$, $Sc_2@C_{84}$, $Sc_3@C_{82}$ and $Sc_4@C_{82}$ [29,30]. It was found that the $Sc_3@C_{82}$ produced ESR-signal but the $Sc_2@C_{82}$ and $Sc_4@C_{82}$ are ESR-silent.

The most abundant endohedral fullerene known so far is the $Sc_3N@C_{80}$ molecule, which was first discovered in 1999 by Stevenson et al [31]. This fullerene is produced by introducing nitrogen gas in the Huffman-Kratschmer chamber where graphite and metal oxide is evaporated in arc-discharge. The most stable $Sc_3N@C_{80}$ has the C_{80} cage in icosahedral symmetry. One important aspect of the $Sc_3N@C_{80}$ is that the neither the Sc_3N cluster nor the I_h- C_{80} cage are stable in isolation. This aspect points to the importance of the charge transfer from the encapsulated unit to the outer cage, which stabilizes the whole molecule. Soon after the discovery of the $Sc_3N@C_{80}$ fullerene, other tri-metallic nitride endohedral fullerenes such as $Er_xSc_{3-x}N@C_{80}$ (x = 0-3) [32] and $A_xSc_{3-x}N@C_{68}$ (x = 0-2; A = Tm, Er, Gd, Ho, La) were also discovered. [33,34,35]

1.3 Non-IPR Endohedral Fullerenes: $A_xSc_{3-x}N@C_{68}$

The geometries of carbon cages are governed by the isolated pentagon rule (IPR), which states that those fullerenes are more stable in which all of the pentagons are surrounded by hexagons and thereby are isolated from each other. [9] However, some of the endohedral fullerenes are found to exhibit non-IPR structure with fused pentagons. One such example is $Sc_2@C_{66}$ where the C_{66} cage cannot have isolated pentagons. We point out that it is not possible for the C_{20}- C_{58}, C_{62}-C_{68} cages to satisfy the isolated pentagon rule. These carbon cages have high strain and as a result are unstable and difficult to isolate. In the endohedral form, however, the complexation releases large strain energy and stable structures

can be formed. One of the carbon cages that show prominent breaking of the isolated pentagon rule in the encapsulated form is the C_{68} e.g. $A_xSc_{3-x}N@C_{68}$ fullerene where x=0-2 and A=Tm, Er, Gd, Ho, La, Sc, $Sc_2C_2@C_{68}$ which are non-IPR fullerenes. [36] However, other cages which can have isolated pentagons were also found to form non-IPR fullerenes when encapsulating a di-metallic cluster e.g. $La_2@C_{72}$. [37]

Apart from the non-IPR structures, the tri-metallic nitride encapsulating C_{68} molecules are interesting also because of their ability to encapsulate a large cluster inside a relatively small cage. Quite a few theoretical and experimental studies have been performed so far on these clusters. [38]. The non-IPR carbon cages have large strain energy from the presence of adjacent pentagons. Re-hybridization of the carbons in the fused pentagonal rings from sp^2 to sp^3 can release the strain energy. This can be achieved through bonding with halide or hydrogen atoms. Another way is through charge transfer from an encapsulated unit. A detailed DFT study was carried out by Chen et al [39]. on the empty C_{68} cage and its anions in charge states -2, -4, and -6. The C_{68} has 6332 isomers and the lowest isomer has C_2 symmetry with 2 adjacent pentagonal rings. The addition of the extra charges stabilizes the cage, however, the energy order of the anionic isomers is different from that of the neutral clusters. The $Sc_3N@C_{68}$ lowest energy structure has D_3 symmetry for the carbon cage whereas the lowest energy empty carbon cage is a different isomer 6140 with C+ symmetry [39]. The Sc_3N unit is found to be in the +6 charge state with six electrons transferred to the carbon cage. Chen et al. have found that while the complexation energy is i.e. the energy released upon formation of the endohedral fullerene is highest for Sc_3N, for other isoelectronic clusters such as Y_3N it is significantly lower. Popov et al. have shown that while C_{68} can encapsulate units like $DySc_2N$, however, $Dy_3N@C_{68}$ does not

occur due to the larger size of the encapsulated cluster [38]. Chen et al. have concluded that the bonding energy for Sc_3N is highest compared to other isoelectronic clusters due to the fact that the Sc_3N is the smallest in size among those. Thus it points to the fact that although the charge transfer from the encapsulated cluster stabilizes the outer carbon cage, the size of the inner unit also plays a crucial role in the stability of the endohedral C_{68} fullerenes.

1.4 $V_xSc_{3-x}N@C_{68}$ Fullerenes: Motivation

Recently, Wei et al. have reported the generation of V containing metal nitride cluster fullerenes $VSc_2N@(I_h\text{-}C_{80})$ and $V_2Sc@(I_h\text{-}C_{80})$ [40] fullerenes and found that the electronic and magnetic properties of such cluster fullerenes can be tuned by tuning the number of V atoms. The vanadium ion can exist in different charge states from +2 to +5 and typically has a small ionic radius that range from 0.46 Å to 0.79 Å. [41] The V atoms are found to be in the +3 charge state with two unpaired d electrons located on each V ion. Since the V atoms have 2 unpaired electrons, these clusters will have a spin state other than a singlet state. This feature can be exploited to generate magnetic cluster fullerenes. One of the questions here is the structure of the tri-metallic nitride C_{68} cluster with a heterogeneous composition of the metal atoms. Moreover, the presence of the V atom will also change the electronic structure, spin state and the optical properties of these clusters. We study these properties of the $VSc_2N@C_{68}$ cluster computationally at the density functional level. In the following section we describe the computational methods used for investigating the properties of these clusters. The results are discussed in the third chapter.

Metallofullerenes made this way include $M@C_{60}$ with M =Li, Ca, Na, K, Rb. However, mostly higher endohedral fullerenes, like $M@C_{82}$, are formed. These metallofullerenes are very stable

molecules and can be used in many applications. For example, it has been shown that the bulk modulus of $K@C_{60}$ is higher than that of C_{60}. From this it can be concluded that for Nano ball-bearing applications, metallofullerenes are more effective than fullerene. A crystal of $La@C_{60}$ is predicted to be an air-stable superconductor since there is a complete charge transfer from La to the C_{60} cage resulting in a triply charged molecule. [42]

Chapter 2: Theory and Methodology

2.1 Density Functional Theory

DFT is a computational quantum mechanical method used to explore the electronic structure of atoms, molecules, clusters, solids to nuclei and quantum fluids. This theory has become popular among the computational chemists, physicists, and material scientists due to low cost of computation and is considered to be accurate in the quantitative aspects. It is successfully employed to study various properties such as structure, potentials, optical, vibrational, electrical, and magnetic properties of materials. The fundamental aspect of DFT is that the ground state properties of a system with many interacting particles are can be determined from spatially dependent ground state electron density and thus the name derived as density functional.

DFT is deeply rooted to the fundamental conceptual framework of the Hohenberg-Kohn theorems. In quantum mechanics the primary goal is to find the complex-valued probability amplitude i.e. the wave function, which contains all the information of a system. Using the wave function, the average values of observables can be calculated using the expectation values of the corresponding operators and thus it is possible to study the system's properties. The time-independent Schrodinger equation for single electron, which is acted upon the external potential $v(\boldsymbol{r})$ (that is an attractive potential by the nucleus) takes the form of

$$\left[\frac{-\hbar^2}{2m}\nabla^2 + v(\boldsymbol{r})\right]\Psi(\boldsymbol{r}) = E\Psi(\boldsymbol{r}),$$

where, E is the energy eigenvalue and m is the mass of the electron. For a system of N interacting electrons acted upon by an external potential $v(\mathbf{r})$, the Schrodinger equation becomes

$$\left[\sum_i^N \left[-\frac{\hbar^2}{2m}\nabla_i{}^2 + v(\boldsymbol{r_i})\right] + \sum_{i<j} U(\boldsymbol{r_i}, \boldsymbol{r_j})\right]\psi(\boldsymbol{r_1}, \boldsymbol{r_2}, \ldots\ldots, \boldsymbol{r_N}) = E\psi(\boldsymbol{r_1}, \boldsymbol{r_2}, \ldots\ldots, \boldsymbol{r_N}),$$

in which the 1st term denotes the kinetic energy operator and remaining two are the potential energy terms. This is a 3N dimensional differential equation and due to the presence of nonlocal electron-electron interaction

$$\widehat{U} = \sum_{i<j} U(\boldsymbol{r_{i,}}, \boldsymbol{r_j}) = \sum_{i<j} \frac{q^2}{|\boldsymbol{r_i} - \boldsymbol{r_j}|} \ ,$$

makes its solution more complicated. In such a situation the 3N dimensional wave function is obtained variationally. The wave-function based methods are accurate depending on the approximations made on the nature of the wave function and are not efficient for complex systems. Unlike the wave function based methods, in density functional theory the central variable is the total electron density of the system. DFT provides a feasible way to solve the Schrodinger equation for the complex systems. DFT is based on the two fundamental theorems of Hohenberg-Kohn, the 1st of which states that the ground state density of a system of N interacting particles is uniquely determined by the external potential ($v(\boldsymbol{r})$). Thus there is a one-to-one mapping between the ground state density and the external potential. This statement is insufficient to trace out the path to choose the true ground state density n($\mathbf{r}$) hence the 2nd H-K theorem has been formulated, which states that total ground state energy of N-electrons system is a functional of ground state electron density (n($\mathbf{r}$)). The second Hohenberg and Kohn theorem thus clearly states that the true ground state electron density will be the one that minimizes the total ground state energy. From H-K theorem the energy functional can be written as a function of single electron density and the expression for the energy functional for a many-body system with is given by

$$E[n] = T[n] + V[n] + U[n]$$

In above expression 1st, 2nd and 3rd terms on the right hand side are respectively kinetic energy, potential energy due to coulomb interaction between electrons and nucleus, and potential energy due to electron-electron interaction. Although the Hohenberg-Kohn theorems provide a formal

way to solve the many-body Hamiltonian but in practice it encounters the problem owing to some of the terms that cannot be expressed as a functional of density.

Kohn-Sham formulation simplified the problem in which the system is modeled in such a way that the interacting electrons system is replaced by non-interacting fictitious particle system such that each particle experiences an average potential due to all the other electrons. This leads to the independent particle equations for non-interacting system. In addition, all the interactions like correlation between the particles and exchange interaction due to quantum effect are included in the exchange correlation functional, which is also a functional of density. Moreover, orbitals are introduced so that the kinetic energy can be expressed in terms of the orbitals. The variational process then leads to a set of equations known as Kohn-Sham equations. By solving the equations, it is possible to find the ground state density and energy of the interacting system in which the accuracy relies on the approximation that has been made during the formulation of the exchange correlation functional. In this formulation the energy functional is expressed in terms of the Kohn-Sham orbitals, which is used to find the kinetic energy and density of the electrons:

$$E[n] = -\frac{\hbar^2}{2m}\sum_i \int \psi_i{}^* \nabla^2 \psi_i d^3\boldsymbol{r} + \int v(\boldsymbol{r}) n(\boldsymbol{r}) d^3\boldsymbol{r} + \frac{e^2}{2}\int\int \frac{n(\boldsymbol{r})n(\boldsymbol{r}')}{|\boldsymbol{r}-\boldsymbol{r}'|} d^3\boldsymbol{r} d^3\boldsymbol{r}' + E_{xc}[n] + E_{ion-ion}$$

In this expression the terms on the right hand side from the left are kinetic energy, potential due to coulomb interaction between electrons and nucleus, potential due to coulomb interaction between electrons, exchange-correlation energy and the last term is due to coulomb interaction between the nuclei. The term $E_{xc}[n]$ covers all the effects that are not included in the first three terms. The last term includes the nuclear-nuclear repulsion energy.

Minimizing the aforementioned expression of energy functional with density leads to the set of equations known as Kohn-Sham equations, which are indicated by

$$\left[-\frac{\hbar^2}{2m}\nabla^2 + v(\boldsymbol{r}) + V_H(\boldsymbol{r}) + V_{XC}(\boldsymbol{r})\right]\psi_i(\boldsymbol{r}) = \varepsilon_i\psi_i(\boldsymbol{r}),$$

in which the potential term v(**r**) is the external potential due to the interaction between electron and nuclei. The Hartee potential is symbolized by

$$V_H(\boldsymbol{r}) = e^2 \int \frac{n(\boldsymbol{r}')}{|\boldsymbol{r}-\boldsymbol{r}'|} d^3\boldsymbol{r}' \ .$$

This is the interaction of an electron with total electron density due to which the interaction of an electron with itself is also included which does not have any physical meaning, so it is necessary to include the correction term together with correlation between electrons in V_{XC} which can be defined as

$$V_{XC}(\boldsymbol{r}) = \frac{\delta E_{XC}(\boldsymbol{r})}{\delta n(\boldsymbol{r})}.$$

In practice, a trial density that integrates to the correct number of electrons is chosen and the potential is calculated and used to solve the Kohn-Sham equations which yield the single electron orbitals. Electron density can be calculated by using

$$n(\boldsymbol{r}) = 2\sum_i \psi_i^*(\boldsymbol{r})\psi_i(\boldsymbol{r}),$$

which can be used to calculate the potential and solve the Kohn-Sham equations iteratively to a desired convergence criterion.

We have used the Generalized Gradient Approximation in our DFT calculation. Among the various GGA functions, we have selected the Predew-Burke-Ernzerhof (PBE) functional and which are implemented in the massively parallel NRLMOL code. [43,44,45,46]

2.2 Ionization Potential

Amount of energy required to remove a single electron from atom, ion, molecule from its ground state so that parent atom left becomes positive left is ionization potential (IP).

The ionization potential (IP) of a neutral molecule (with N electrons) is given by the following expression:

$$IP = E_{N-1} - E_N$$

Where E_N is the total energy of the molecule in its ground state and E_{N-1} is the total energy of the cation. The vertical IP refers to the energy of the cation at the geometry of the neutral molecule.

Orbital study of atoms gives the information about the frontier orbitals, Which are highest occupied molecular orbital (HOMO) and lowest unoccupied molecular orbital(LUMO). HOMO is the outermost orbital containing an electron. The LUMO is the first immediate orbital after HOMO that does not contain an electron. Ionization energy also can be defined according to Koopmans's theorem: The energy corresponding to HOMO is also called Ionization Energy.

2.3 Electron Affinity

Electron Affinity is the amount of energy released when an electron is added to the system so that atom becomes a negative ion. The chemical equation to represent the electron affinity (EA) of a neutral molecule (with N electrons) is calculated by the expression:

$$EA=E_N - E_{N+1}$$

E_{N+1} is the total energy of the anions. Similar to the vertical IP, the vertical EA is obtained by using the geometry of the neutral molecule for the anion.

2.3 Joint Density of States

The joint density of states is proportional to the number of possible optical transitions between electronic states associated in the valence band and electronic states associated with the conduction band, separated with energy by a fixed energy. The number of energy states in the two bands, where transitions are possible can be calculated by joint density of states. So, it gives the threshold transition where abortions are possible to transfer the electrons from certain energy range to the next levels. It helps to calculate only those transition which are allowed.

Chapter 3: Results and Discussion

The computational search for the lowest few isomers of $VSc_2N@C_{68}$ is a daunting task due to the fact that the fullerene cage has 6332 isomers. Further the orientation of the encapsulated cluster can vary for a given cage, which makes the search for lowest energy structure computationally expensive. Since the V atoms are found to be in the +3 state in the $VSc_2N@C_{68}$ fullerene [47], the number of electrons transferred from the encapsulated cluster to the outer cage is same as that for the Sc_3N cluster. The energy order of the empty neutral carbon cage is different from that of the charge cage and therefore we have examined the stability of the C_{68} isomers in the hexa-anionic state. The preliminary screening was done using the PM6 method using the MOPAC2009 code and the lowest 300 structures were chosen for further analysis. The lowest energy hexa-anionic structure was found to be 6140 isomers with D_3 symmetry. The VSc_2N unit was placed at the center of each of these lowest 300 structures. The VSc_2N unit is planar and therefore we have it perpendicular to three mutually orthogonal directions taken as X, Y, and Z axis that led to 3 different structures for each of the 300 isomer of the anionic cage. These operations led to the generation of a total of 900 isomers of $VSc_2N@C_{68}$. These 900 isomers were optimized at the PM6 level. We point out that some of the rotations did not lead to any change of total energy at the PM6 level. We have chosen the lowest 13 energetically distinct isomers for further optimization with density functional theory. The lowest isomer of the $VSc_2N@C_{68}$ at the PM6 level is the 6140 isomer for C_{68}. The optimized 13 structures are shown below.

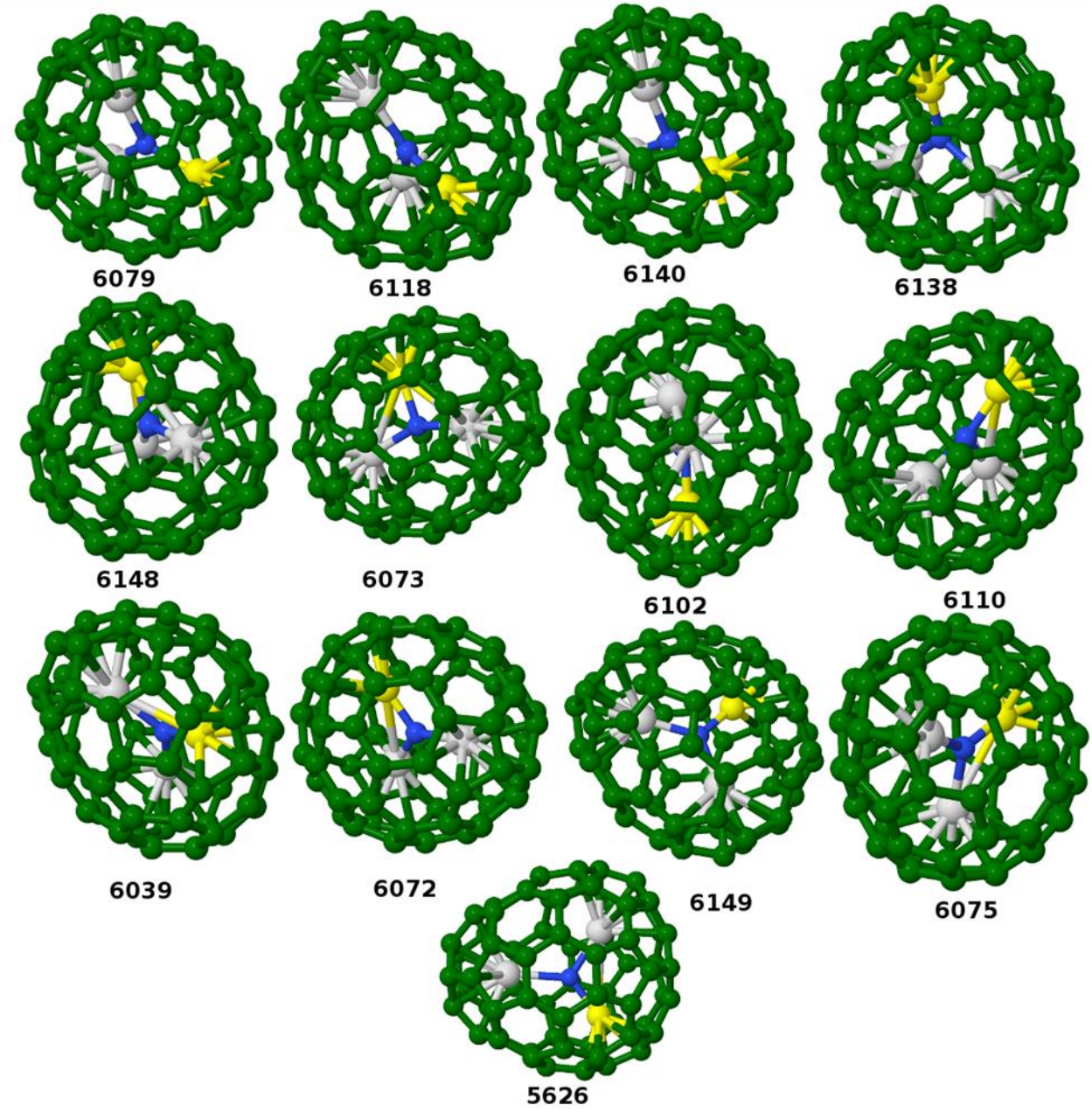

Figure 3.1: Optimized Structures of $VSc_2N@C_{68}$ isomers

Chen et al. [47] have earlier carried out a similar calculation with PM3 method for optimization of C_{68} isomers with particular symmetry followed by DFT calculations for various anionic states with charges q=-2, -4, and -6. The DFT calculations were

done using the B3LYP functional for exchange-correlation energy. Their results indicate that the lowest energy structures for the anionic clusters are same at both PM3 and DFT- B3LYP level. They have found that the lowest isomer of the C_{68} in the hexa-anionic state is the isomer 6140 that has D3 symmetry with three pairs of adjacent pentagons. The same cage isomer was also identified as the structure of the $Sc_3N@C_{68}$ fullerene by X-ray crystallography and NMR spectroscopy. [48] This result is in agreement with our PM6 calculations on the hexa-anionic C_{68} cages and also on $VSc_2N@C_{68}$ cage. However, at the DFT level, we find that the order of the $VSc_2N@C_{68}$ is different from that obtained with the PM6 method. The lowest 13 isomers of the empty C68 fullerene in the hexa-anionic state are presented in Table 3.1. At the DFT level, the isomer 6079 is the lowest energy structure.

Table 3.1: Relative Optimized Ground State Energy and adjacent Pentagons

Isomers	Relative Ground State Energy (eV)		Adjacent Pentagons	
	DFT	PM6	2 Pentagons	3 Pentagons
6079	0	0.317	2	1
6118	0.457	0.258	4	0
6140	0.538	0	3	0
6138	0.852	0.405	3	0
6148	0.855	0.778	2	0
6073	0.991	0.675	2	0
6102	1.035	0.27	3	0
6110	1.08	0.442	3	0
6039	1.262	0.432	3	0
6072	1.288	0.512	3	0
6149	1.342	0.461	2	0
6075	1.483	0.625	3	0
5626	1.85	0.492	2	1

The isomer 6079 has C3 symmetry but with two pairs of adjacent pentagons and one with three adjacent pentagons which indicates high strain on the cage. It is known that highly charged cages often adapt structures that are realizable only under strain. We find that the metal atoms are pointing to the 5:5 C-C bonds of the adjacent pentagons. The V-N bond is 1.94 Å which is shorter than the other two Sc-N bonds which are 2.06 Å long. Thus due to the substitution also

the symmetry of the molecule is lowered. The $Sc_3N@C_{68}$ lowest energy isomer had D3 symmetry.

The distance between the V and the nearest carbon on the cage is 2.13 Å. In the $VSc_2N@C_{68}$ whereas the distance between the Sc and the closest C atom is 2.34 Å. The $VSc_2N@C_{68}$ isomers are also energetically quite distinct with the next low-lying isomer at 0.46 eV above. We also find that the isomer 6138 and 6148 are energetically very close to each other but are structurally different. While the rotation of the VSc_2N unit about the C3 axis does not change the total energy at the PM6 level, the rotation through an axis perpendicular to the C3 axis changes it by only 0.13 kcal/mol. It is reasonable that the endohedral unit follows the symmetry of the carbon cage. In the $Sc_3N@C_{80}$ the endohedral unit is free to rotate inside the C_{80} cage, which has much higher symmetry and larger radius.

One of the indicators of the chemical stability of a cluster is the energy gap between the highest occupied molecular orbital and the lowest unoccupied molecular orbital – better known as HOMO-LUMO gap. The density functional theory cannot determine the HOMO-LUMO gap correctly due to the inherent self-interaction errors, which push up the occupied orbitals in energy. However, the HOMO-LUMO gap can be estimated from the difference between the ionization potential and electron affinity, which is called the quasi-particle gap. We present the HOMO-LUMO gaps as directly calculated within the PBE approximation and also the vertical IP, EA and the quasi-particle gaps for all the isomers studied here. The vertical IP or EA assumes that the ionization process is instantaneous and the molecule does not relax. The lowest energy structure has a small HOMO-LUMO gap of 0.31 eV calculated at the GGA-PBE level. The vertical ionization potential of the isomer 6079 is 6.12 eV, which is smaller than that of C60. The vertical electron affinity is 2.32 eV, but the adiabatic electron affinity of 2.64 eV is close to that

of C60. The calculated quasi-particle gap thus is 3.48 eV. The large gap signifies chemically stability. The high electron affinity indicates that the $VSc_2N@C_{68}$ can potentially be a good electron acceptor. However, for applications in devices such as photovoltaics other factors are also important such as the reorganization energy and charge mobility.

Table 3.2: HOMO-LUMO, Vertical IP and EA with Quasi-Particle Gap

Isomers	HOMO - LUMO Gap (eV)	Vertical Ionization Potential (eV)	Vertical Electron Affinity (eV)	Quasi - Particle Gap (eV)
6079	0.305	6.121	2.319	3.802
6118	0.373	5.897	2.360	3.537
6140	0.324	5.610	2.490	3.120
6138	0.314	5.933	2.535	3.398
6148	0.350	6.038	2.376	3.662
6073	0.426	6.131	2.808	3.323
6102	0.311	5.844	2.455	3.389
6110	0.356	6.087	2.250	3.837
6039	0.419	6.451	2.214	4.237
6072	0.399	6.201	2.371	3.830
6149	0.729	6.198	2.589	3.609
6075	0.061	5.883	2.524	3.359
5626	0.410	5.797	2.234	3.563

Several of the $VSc_2N@C_{68}$ isomers have spin moment of 2 μB which arises from the incompletely filled d-orbitals of the vanadium ion. The vanadium and the scandium ions are in the +3 charge state leading to 2 d-electrons on the V ion. The VSc_2N cluster is in the +6 charge state. The density of states (DOS) of the lowest energy isomer of $VSc_2N@C_{68}$ (6079) is shown in Fig.3.2.

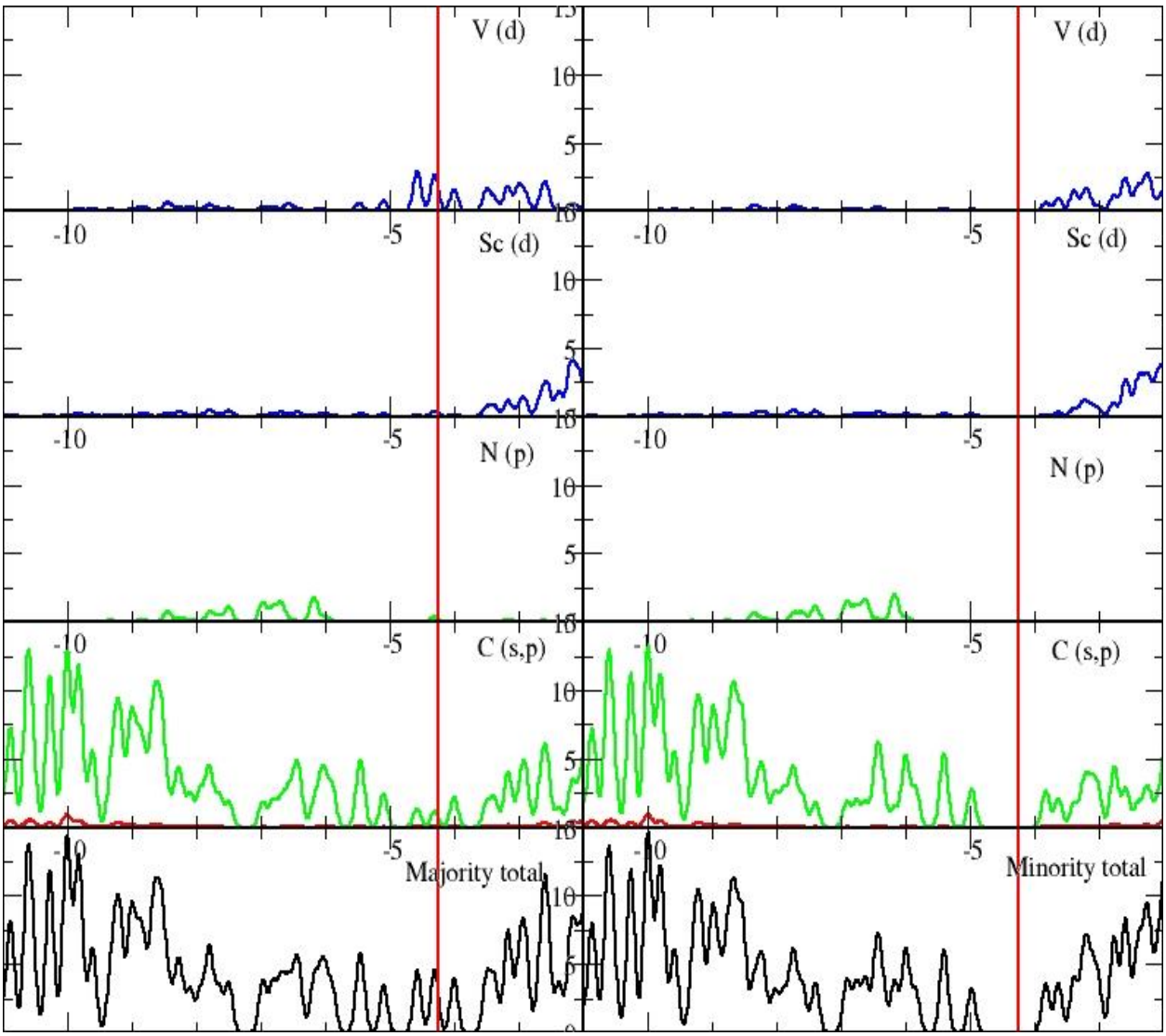

Figure 3.2: Orbital DOS plot of the lowest Energy isomer of $VSc_2N@C_{68}$

The DOS plot shows the majority d-electrons on the V atom responsible for the overall spin moment of the molecule. Both the HOMO and HOMO-1 orbitals of the molecule have strong d-character arising from the d-orbitals of the V atom as well as contributions from the carbon p orbitals. The LUMO orbital also shows d-character of the same spin. The wave function to show the contribution of d -orbitals to HOMO, HOMO-1 and LUMO of 6079 are shown in the fig below.

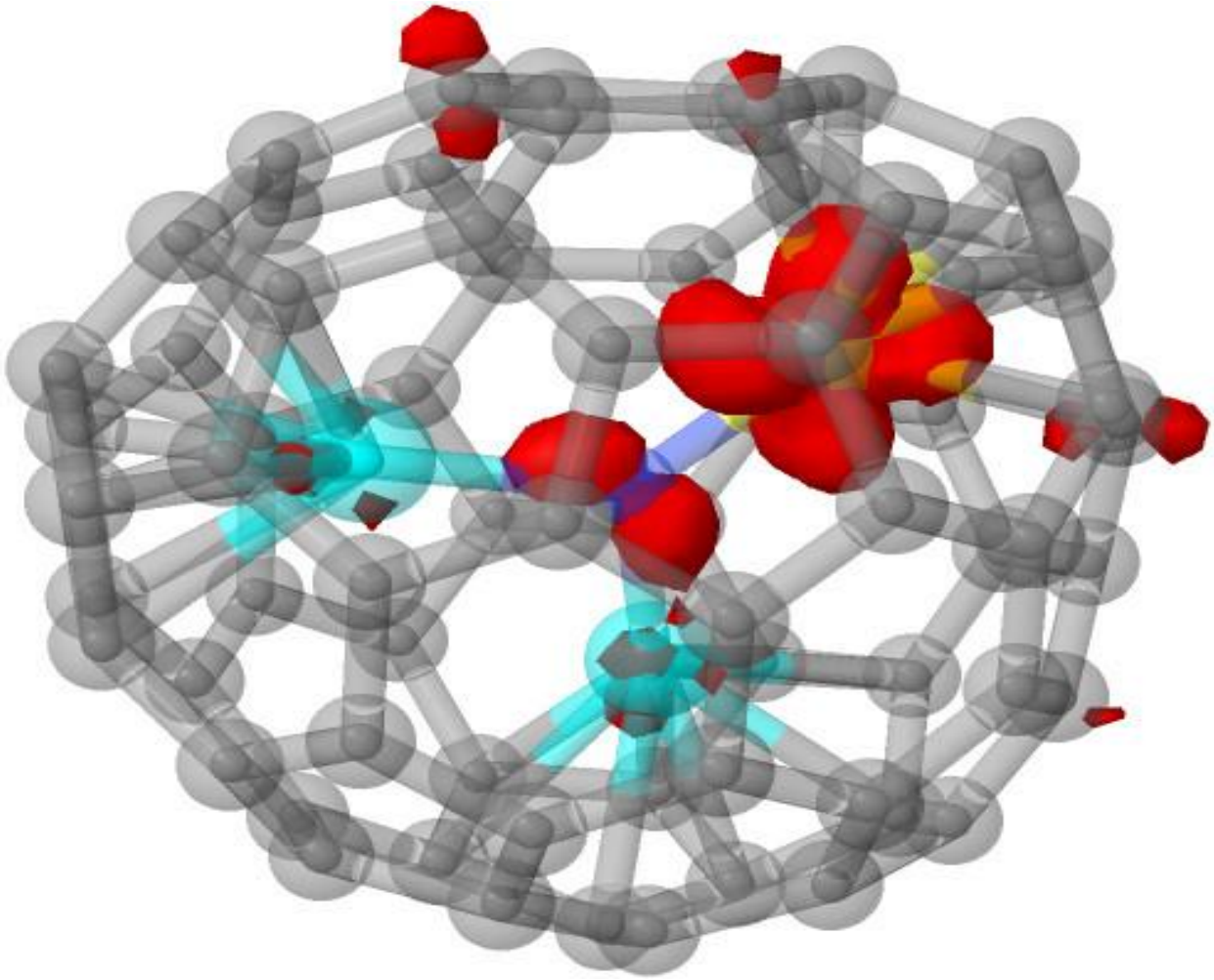

Figure 3.3: HOMO of 6079

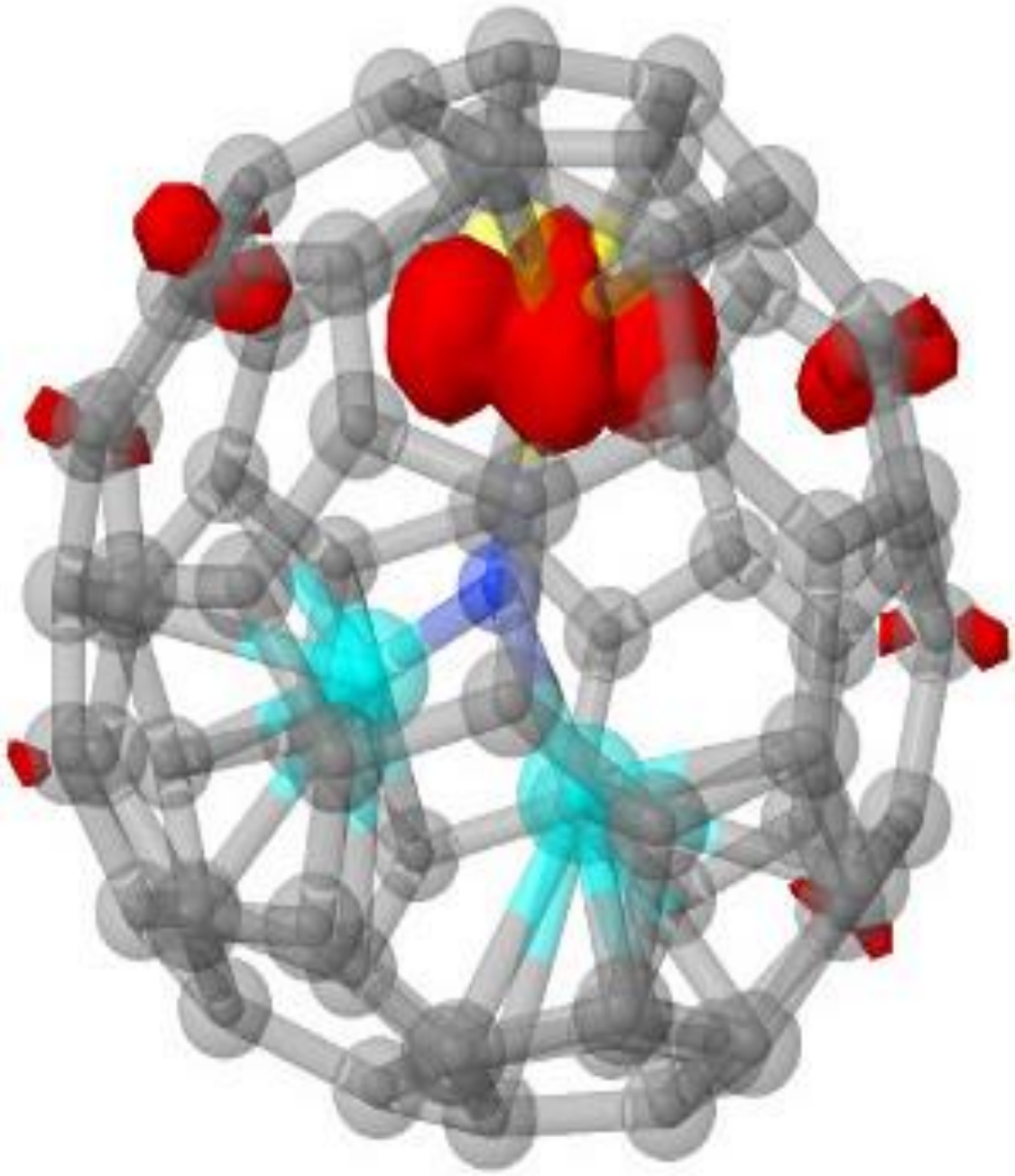

Figure 3.4: HOMO-1 of 6079

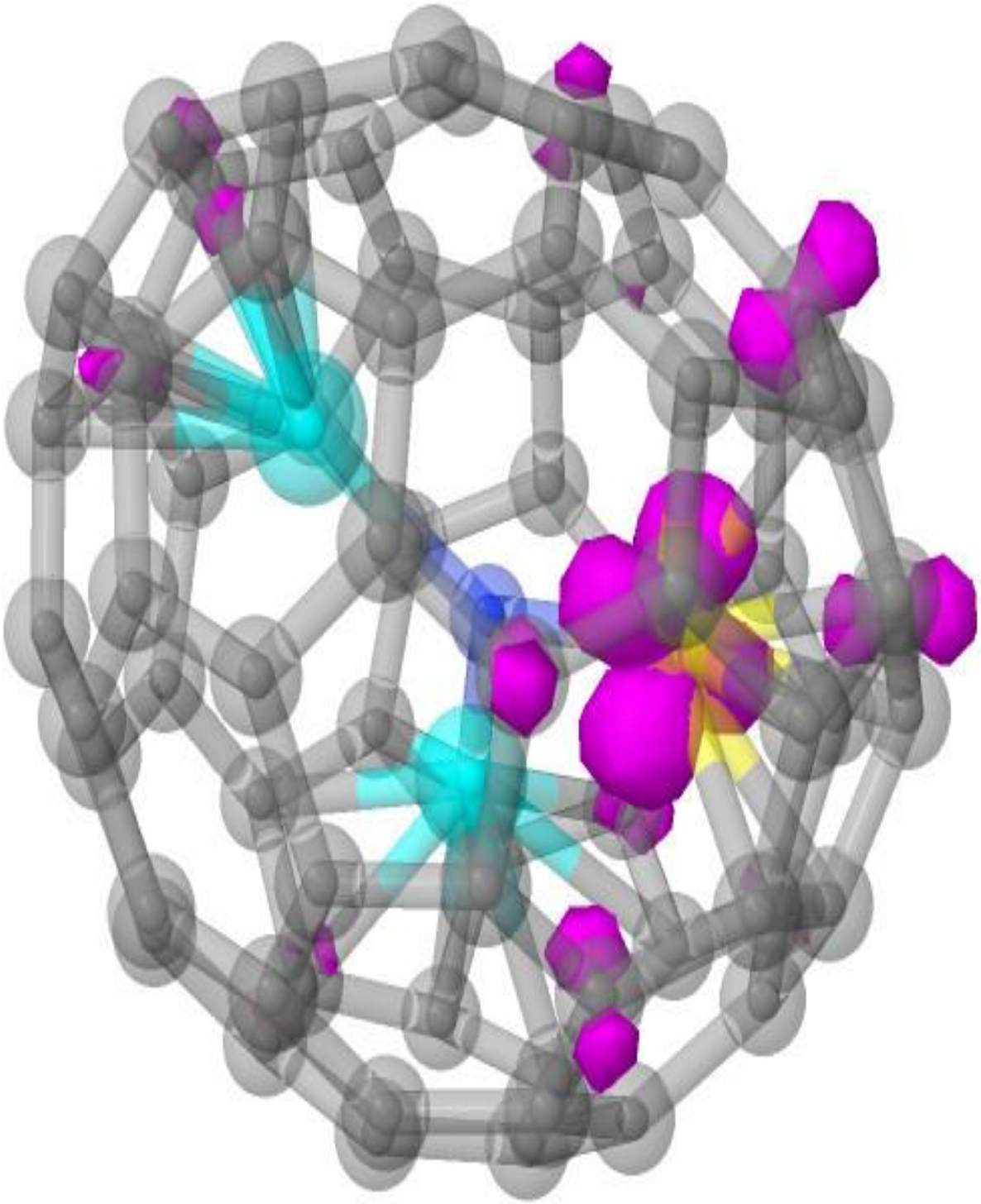

Figure 3.5: LUMO of 6079

Similar spin moment is also present in the isomers 6072 and 6149. In the rest of the isomers, the spin magnetic moment is 0. We examined the DOS of the isomer 6140 to understand the difference in the DOS between the spin compensated S=0 isomer 6079 and S=1 isomer 6140. The isomer 6140 is remarkably similar to the isomer 6079 but with significantly different electronic structure. The HOMO of the isomer 6140, has strong d-character, but is completely filled. The LUMO also has prominent d-orbital contributions but the HOMO-1 in this isomer arises mainly from carbon 2p orbitals. The V-N bond in the isomer 6140 is shorter at 1.86 Å but the C-V distance is also slightly lower at 2.09 Å. The field effect of the cage is likely to be higher which introduces higher splitting of the d-levels leading to filling of the d orbital resulting in zero spin density on the V atom. To rule out the possibility of the V atom being in a different charge state, we have also calculated the total charge in a sphere of radius 2.3 Bohr around the V atom. The calculated charge in both the isomer 6140 and 6079 is same but the integrated spin charge is different. This result indicates that in both the molecules the V atoms are in similar charge states but in different spin states. This result brings out the influence of the cage on the encapsulated unit.

The joint density of state plot of most optimized structure of isomer is found as shown in the graph 3.6, which describes the optical absorption spectrum. There are couple of peaks before the one with maximum intensity at the peak at the energy value 3.49 eV. Here we are mainly interested in the maximum peak is the most probable at which the more transition takes place.

The Joint density of states plot for VSc2N@C68:6079 is shown in graph 1. This describes the optical absorption spectra of the given isomer. The transition corresponding to the four major projections give the absorption spectra with the respective energy. The major peaks are at 1.05, 1.6, 2.7 and 3.49 eV taken to discuss the nature of transition state.

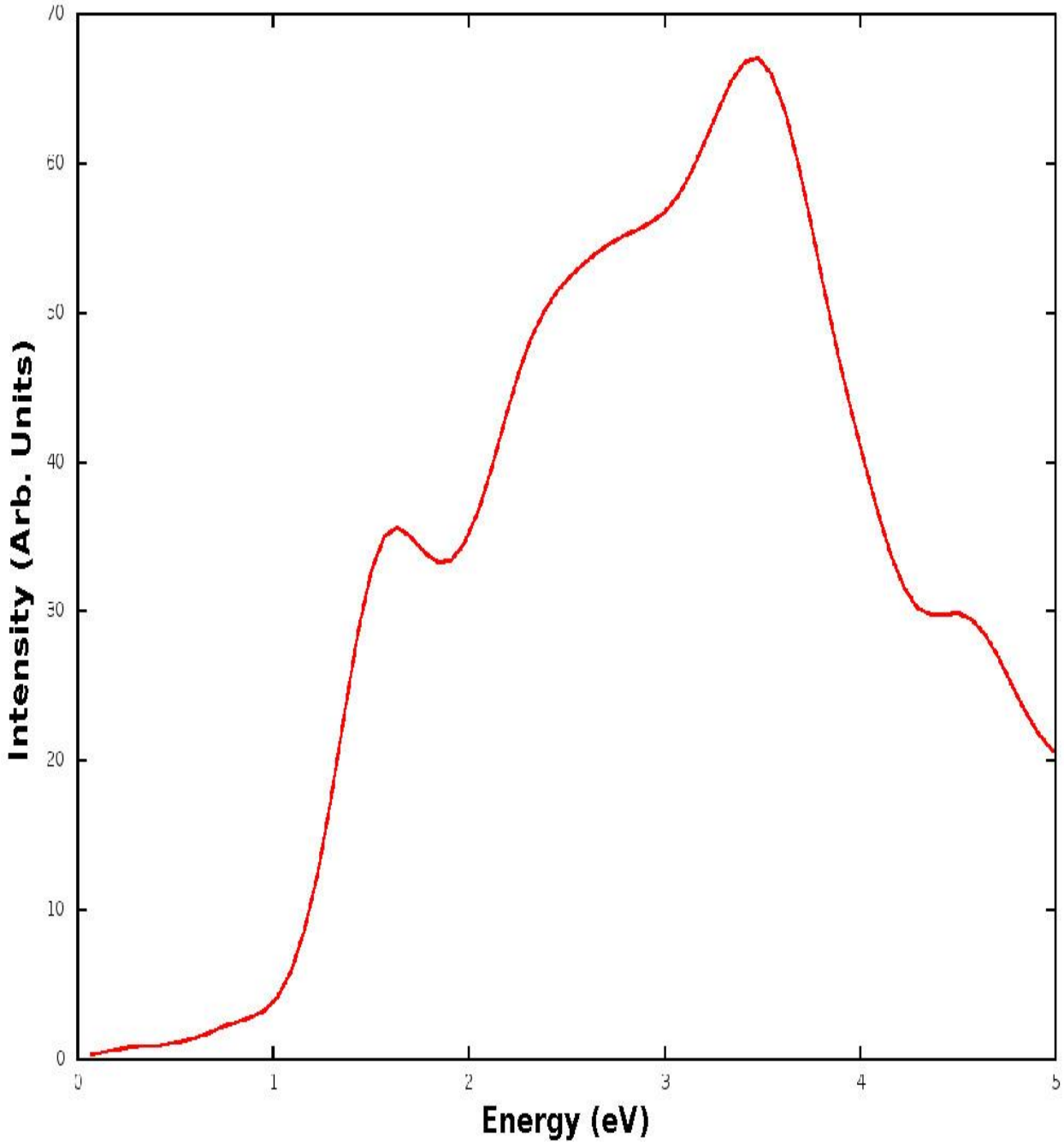

Figure 3.6: Joint Density of States of $VSc_2N@C_{68}$:6079

The transition corresponding to different energy states are tabulated below. The spin 1 represents majority and 2 represents minority electrons.

Table 3.3: Allowed transition corresponding to different energy

Energy: 1.05 eV					
Ei	Ej	Transition		Spin	Intensity
		From	To		
-0.158	-0.116	H	L-9 (5)	1	0.221
-0.168	-0.124	H-1 (1)	L+5 (3)	1	0.76
Energy:1.6 eV					
-0.187	-0.128	H-3	L+3	1	0.91
-0.158	-0.098	H	L+17 (10)	1	0.162
Energy: 2.7 eV					
-0.216	-0.116	H-9 (5)	L+9 (5)	1	1.118
-0.245	-147	H-23 (12)	L	1	0.636
Energy: 3.49 eV					
-0.199	-0.07	H-5 (3)	L+37 (20)	2	1.18
-0.22	-0.093	H-11 (6)	L+22 (13)	2	1.292
-0.22	-0.093	H-11 (6)	L+22 (13)	2	1.315
-0.245	-0.116	H-23 (12)	L+9 (5)	1	0.353
-0.254	-0.125	H-26 (13)	L+4	2	0.125
-0.275	-0.147	H-29 (15)	L	1	0.155

The peak corresponding to the energy at 1.05 eV which is mainly due to the transitions from HOMO to L+5 and HOMO-1 to LUMO+3 for majority electrons. Those transitions are

mostly contributed by the excitation from d orbital of Vanadium to p-orbital carbon and d-orbitals of Vanadium to d- orbital of Sc.

In the second projection corresponding to 1.6 eV, possible transition that takes place are also due to majority electrons. The transition that takes place from HOMO-3 to LUMO+3 and HOMO to LUMO+10 are due to transfer of electrons from occupied d-orbitals of V to the unoccupied p-orbitals of Carbon.

For the energy at third peak at 2.7 eV, transitions are still due to majority electrons. With the energy corresponding to 2.7 eV, there are two transitions possible which are from HOMO-5 to LUMO+5 and HOMO-12 to LUMO. It takes place from p-orbitals of Carbon to d-orbitals of Scandium and p-orbitals of Scandium to d-orbitals within the same atom respectively.

The maximum peak in the curve corresponds to energy 3.49 eV. The transition is more with this value than other three energies. The transition that takes place are mainly from p-orbitals Carbon, Scandium and Nitrogen to p-orbitals of Carbon and d-orbitals of Vanadium. In this case the transitions are due to both majority and minority electrons.

Chapter 4: Conclusion

A computational DFT study was carried out on the spin polarized $VSc_2N@C_{68}$ fullerene. The endohedral unit is planner even the rotation of it in 3 different orientations did not make significant change in optimized energy. The results demonstrated that $VSc_2N@C_{68}$:6079 with two pairs of fused pentagons and one set of triply fused pentagons is the most stable isomer. The 6079 isomer has C3 symmetry. Metal atoms inside are pointing to the 5:5 C-C bonds of the adjacent pentagons. The V-N bond is 1.94 Å which is shorter than the other two Sc-N bonds which are 2.06 Å long. Thus due to the substitution the symmetry of the molecule is lowered. The $VSc_2N@C_{68}$ isomers are also energetically quite distinct with the next low-lying isomer at 0.46 eV above. The results obtained also showed that $VSc_2N@C_{68}$ can be a good electron acceptor. Moreover, The Density of State calculation showed that mainly the d electrons of V and p electron of C are responsible for overall HOMO-LUMO gap. The large gap signified that it is chemically stable. The joint density of states calculation shows the optical absorption spectrum with a high peak at 3.49 eV. This result can help in experimental characterization on $VSc_2N@C_{68}$.

References

1. Walton, H. W. Korto, D. R. M., The fullerenes, New Horizons for the Chemistry, Physics and Astrophysics of Carbon, Cambridge University Press.
2. Curl, R. F. Dawn of the fullerenes, experiment and conjecture. Mod. Physics 69,1997, 691-702.
3. W. J. Anton, R. W. Stephen, I. S. David, Biological Applications of Fullerenes. New York City, NY: Elsevier Science, 1996.
4. M. Prato, J. Mater. Chem. 1 (1997) 1097.
5. E. G. Galpern, I. V. Stankevich, A. L. Chistyakov, and L. A. Chernozatonskii, Fullerene Sci. Technol.2,1(1994).
6. Koeppe R., Sariciftci N. S., Photoinduced charge and energy transfer involving fullerene derivatives Photochem. Photobiol Scie.5, 2006, 1122-31.
7. Zanasi. R., and Fowler, P. W., Chem. Phys. Lett. 238,270 (1995).
8. A. Sassara, G. Zerza, M. Chergui, Absorption Wavelengths and Bandwidths for Interstellar Searches of C60 in the 2400–4100 Å Region, The Astrophysical Journal Supplement Series, 135:263-273, 2001 August.
9. L.S. Wang, C. Conceicao, C. Jin, R.E. Smalley, Chem. Phys. Lett. 182 (1991) 5.
10. O.V. Boltalina, I.N. Ioffe, I.D. Sorokin, L.N. Sidorov, J. Phys.Chem. 101 (1997) 9561.
11. A. F. Hebard, M. J. Rosseinsky, R. C. Haddon, D. W. Murphy, S. H. Glarum, T. T. M. Palstra, A. P. Ramirez and A. R. Kortan, Nature, 350 (1991) 600.
12. N. Tezuka, T. Umeyama, S. Seki, Y. Matano, M. Nishi, K. Hirao, H. Lehtivuori, N. V. tkaxhenko, H. Lemmetyinen, Y. Nakao, S. Sakaki, H. Imahori, Comparision of cluster

formation, film structure, microwave conductivity and photochemical properties of composites consisting single walled carbon nanotubes with C_{60}, C_{70} and C_{84}, 2010, Journal of Phys. Chemistry C, 114,3235-3247.

13. H. W. Kroto, Nature 1987, 329, 529–531.
14. S. Xie, F. Gao, X. Lu, R. Huang, C. Wang, X. Zheng, M. Liu, S. Deng, L. Zheng, Science 2004, 304, 699.
15. H.W. Kroto, J.R. Heath, S.C. Obrien, R.F. Curl, R.E. Smalley, Nature 318 (1985) 162.
16. J. R. Heath, S.C. O'Brien, Q. Zhang, Y. Liu, R.F. Curl, F. K. Tittel, R.E. Smalley, Lanthanum complexes of spheroidal carbon shells, Journal of the American Chemical Society 107 (25).
17. W. Krätschmer , K. Fostiropoulos , Donald R. Huffman, The infrared and ultraviolet absorption spectra of laboratory-produced carbon dust: evidence for the presence of the C_{60} molecule, Chemical Physics Letters 170(2) (1990) 167-170.
18. W. Kratschmer, L D. Lamb, K. Fostiropoulos, D. R. Huffman, Solid C_{60}: a new form of carbon, Nature 347 (6291) (1990) 354-358.
19. Koltover, V.K. Endohedral fullerenes: from chemical physics to nanotechnology and nanomedicine. In: "Progress in Fullerene Research" (Ed. M. Lang), New York: Nova Science Publishers, 2007, pp. 199-233.
20. M Saunders, H A. Jiménez-Vázquez1, R. J. Cross, R. J. Poreda, Stable Compounds of Helium and Neon: He@C_{60} and Ne@C_{60}, Science 259 (5100) (1993) 1428-1430.

21. M. Saunders, H. A. Jimenez-Vazquez, R. J. Cross, S. Mroczkowski, M. L. Gross, D. E. Giblin, R. J. Poreda, Incorporation of helium, neon, argon, krypton, and xenon into fullerenes using high pressure, Journal of the American Chemical Society 116 (5) (1994) 2193-2194.

22. T. A. Murphy, T. Pawlink, A. Weidinger, M. Hohne, R. Alcala, J.M. Spaeth, Observation of atomlike nitrogen in nitrogen-implanted solid C_{60}, Phys. Rev. Lett. 77 (1996) 1075-1078.

23. M. Waiblinger, K. Lips, W. Harneit, A. Weidinger, E. Dietel, A. Hirsch, Corrected Article: Thermal stability of the endohedral fullerenes N@C60, N@C70, and P@C60 [Phys. Rev. B **63**, 045421 (2001)].

24. Y. Chai, T. Guo, C. Jin, R. E. Haufler, L. P. F. Chibante, J. Fure, L. Wang, J. M. Alford, R. E. Smalley, Fullerenes with metals inside, The Journal of Physical Chemistry 95 (20) (1991) 7564-7568.

25. J. H. Weaver, Y. Chai, G.H. Kroll, C. Jin, T. R. Ohno, R. E. Haufler, T. Guo, J. M. Alford, J. Conceicao, L. P. F. Chibante, A. Jain, G. Palmer, R.E. Smalley, XPS probes of carbon-caged metals, Chemical Physics Letters 190 (5) (1992) 460-464.

26. S. W. McElvany, Production of endohedral yttrium-fullerene cations by direct laser vaporization, The Journal of Physical Chemistry 96 (12) (1992) 4935-4937.

27. H. Shinohara, H. Sato, Y. Saito, M. Ohkohchi, Y. Ando, Mass Spectroscopic and esr Characterization of soluble Yttrium- containing metallofullerenes yc82 and y2c82, The Journal of Physical Chemistry 96 (9) (1992) 3571-3573.

28. E. G. Gillan, C. Yeretzian, K.S. Min, M. M. Alvarez, R. L. Whetten, R. B. Kaner, Endohedral rare-earth fullerene complexes, The Journal of Physical Chemistry 97 (26) (1993) 6801-6805.

29. C. S. Yannoni, M. Hoinkis, M. S. de Vries, D. S. Bethune, J. R. Salem, M. S. Crowder, R. D. Johnson, Scandium cluster is fullerene cages, Science 256 (5060) (1992) 1191-1192.
30. H. Shinohara, H. Sato, M. Ohkohchi, Y. Ando, T. Kodama, T. Shida, T. Kato, Y. Saito, Encapsulation of a scandium trimer in C_{82}, Nature 357 (6373) (1992) 52-54.
31. S. Stevenson, G. Rice, T. Glass, K. Harich, F. Cromer, M. R. Jordan, J. Craft, E. Hadju, R. Bible, M. M. Olmstead, K. Maitra, A. J. Fisher, A. L. Balch, H. C. Dorn, Small-bandgap endohedral metallofullerenes in high yield and purity, Nature 401 (6748) (1999) 55-57.
32. M. M. Olmstead, A. de Bettencourt-Dias, J. C. Duchamp, S. Stevenson, H. C. Dorn, and A. L. Balch, Isolation and Crystallographic characterization of ersc2n@C-80, Journal of the American Chemical Society., 122, (49) (2000) 12220-12226.
33. H. C. Dorn, S. Stevenson, J. Craft, F. Cromer, J. Duchamp, G. Rice, T. Glass, K. Harich, P. W. Fowler, T Heine, E. Hajdu, R. Bible, M. M. Olmstead, K. Maitra, A. J. Fisher, A. L. Balch, the encapsulation of tri-metallic nitride clusters in fullerene cages, Electronic Properties of Novel Materials-Molecular Nanostructures 544 (2000) 135-141.
34. M. M. Olmstead, H. M. Lee, J. C. Duchamp, S. Stevenson, D. Marciu, H. C. Dorn, A. L. Balch, Sc3N@C68: Folded pentalene coordination in an endohedral fullerene that does not obey the isolated pentagon rule, Angewandte Chemie-International Edition 42 (8) (2003).
36. S. Stevenson, P. W. Fowler, T. Heine, J. C. Duchamp, G. Rice, T. Glass, K. Harich, E. Hajdu, R. Bible, H. C. Dorn, Materials science – a stable non -classical metallofullerene family, Nature 408 (6811) (2000) 427-428.
37. S. Yang, A. A. Popov, L. Dunsch, Large mixed metal nitride clusters encapsulated in a small cage: the confinement of the C68-based clusterfullerenes, Chem. Commun. (2008) 2885-2887.

38. S. Stevenson, P. W. Fowler, T. Heine, J. C. Duchamp, G. Rice, T. Glass, K. Harich, E. Hajdu, R. Bible, and H. C. Dorn, Nature, 408, 427 (2000)

39. H. Kato, T. Taninaka, T. Sugai, and H. Shinohara, J. Am. Chem. Soc., 125, 7782 (2003)

40. D. L. Chen, W. Q. Tian, J. K. Feng, C. C. Sun, C68 Fullerene Isomers, Anions, and their Metallofullerenes: Charge-Stabilizing Different Isomers, Chem PhysChem 9 (3) (2008) 454-461.

41. T. Wei, S. Wang, X. Lu, Y. Tan, J. Huang, F. Liu, Q. Li, S. Xie, S. Yang, Entrapping a Group-VB Transition Metal, Vanadium, within an Endohedral Metallofullerene: VxSc3–xN@Ih-C80 (x = 1, 2), Journal of the American Chemical Society 138 (1) (2016) 207-214.

42. Shannon R. D. A. Crystallogr, Sect. A: Cryst. Phys., Diffr., Theor. Gen. Crystallogr. 1976, A32, 751, DOI: 10.1107/S0567739476001551.

43. D. Lothar, Y Shangfeng, The recent state of endohedral fullerene research, â€ The Electrochemical Society Interface, Summer, 2006

44. M. R. Pederson, K. A. Jackson, Variational mesh for quantum mechanical simulations, Physical Review B. Condensed Matter 41 (11) (1990) 7453-7461.

45. K. Jackson, M. R. Pederson, Accurate forces in a local-orbital approach to the local density approximation, Physical Review B. Condensed Matter 42 (6) (1990) 3276-3281.

46. D. Porezag, M. R. Pederson, Infrared intensities and raman scattering activities within density functional theory, Physical Review B. Condensed Matter 54 (11) (1996) 7830-7836.

47. D. Porezag, M. R. Pederson, Optimization of Gaussian basis sets for density functional calculations, Physical review a 60 (4) (1999) 2840-2847.

48. DL Chen, WQ Tian, JK Fang, CC Sun, C68 fullerene isomers, anions, and their metallofullerenes: charge-stabilizing different isomers, Chemphyschem.,2008 Feb 22, 9(3):454-61.

Vita

Surendra Bhatta was born in Nawalparasi, Nepal. He is the son of Ram Prasad Bhatta and Dev Maya Bhatta. He has graduated Master's degree in Physics from Tribhuvan University, Nepal. He joined the University of Texas at El Paso in 2014.

Permanent address: 3500 Sun Bowl Dr
Apt # 10, El Paso
TX, 79902

Email: sbhatta@miners.utep.edu

The author typed the thesis.